Advances in Radiation Oncology (2017) **2**, 475-484

advances
in radiation oncology

www.advancesradonc.org

Scientific Article

# Detection of regional radiation-induced lung injury using hyperpolarized $^{129}$Xe chemical shift imaging in a rat model involving partial lung irradiation: Proof-of-concept demonstration

**Brandon Zanette MSc [a,b,*], Elaine Stirrat BSc [b], Salomeh Jelveh MSc [c], Andrew Hope MD [c,d], Giles Santyr PhD [a,b]**

[a] *Department of Medical Biophysics, University of Toronto, Toronto, Ontario*
[b] *Physiology & Experimental Medicine Program, Peter Gilgan Centre for Research and Learning, The Hospital for Sick Children, Toronto, Ontario*
[c] *Radiation Medicine Program, Princess Margaret Cancer Centre, Toronto, Ontario*
[d] *Department of Radiation Oncology, University of Toronto, Toronto, Ontario*

Received 25 January 2017; accepted 19 May 2017

**Abstract**

**Purpose:** The purpose of this work was to use magnetic resonance imaging (MRI) of hyperpolarized (HP) $^{129}$Xe dissolved in pulmonary tissue (PT) and red blood cells (RBCs) to detect regional changes to PT structure and perfusion in a partial-lung rat model of radiation-induced lung injury and compare with histology.

**Methods and materials:** The right medial region of the lungs of 6 Sprague-Dawley rats was irradiated (20 Gy, single-fraction). A second nonirradiated cohort served as the control group. Imaging was performed 4 weeks after irradiation to quantify intensity and heterogeneity of PT and RBC $^{129}$Xe signals. Imaging findings were correlated with measures of PT and RBC distribution.

**Results:** Asymmetric (right vs left) changes in $^{129}$Xe signal intensity and heterogeneity were observed in the irradiated cohort but were not seen in the control group. PT signal was observed to increase in intensity and heterogeneity and RBC signal was observed to increase in heterogeneity in the irradiated right lungs, consistent with histology.

**Conclusion:** Regional changes to PT and RBC $^{129}$Xe signals are detectable 4 weeks following partial-lung irradiation in rats.



Supplementary material for this article (http://dx.doi.org/10.1016/j.adro.2017.05.005) can be found at www.advancesradonc.org.

Sources of support: This work was supported by an NSERC Discovery grant (RGPIN 217015-2013) and a CIHR operating grant (MOP 123431).
Conflicts of interest: None.

* Corresponding author. Peter Gilgan Centre for Research and Learning, The Hospital for Sick Children, 686 Bay St., Toronto, ON, Canada M5G0A4.
*E-mail address:* brandon.zanette@sickkids.ca (B. Zanette)

http://dx.doi.org/10.1016/j.adro.2017.05.005

## Introduction

Radiation therapy (RT) is an important treatment modality for thoracic cancers. Unfortunately, radiation-induced lung injury (RILI) may occur in as much as approximately 33% of cases, although the reported incidence varies significantly.[1-6] Risk of RILI remains the main limitation in RT dose prescription and delivery, posing a significant problem for cancer management. RILI typically manifests in 2 stages after RT: (1) an early (weeks to months) inflammatory stage known as radiation pneumonitis (RP) and (2) a late (months to year) stage known as radiation fibrosis (RF). RP is characterized by inflammation of the lung interstitium, destruction of type I pneumocytes, edema of alveoli, and vascular thrombosis and remodelling.[1,5,7] These contribute to an overall decline in lung function and inhibition of gas exchange between the airspaces of the alveoli and capillaries. Early RP is potentially reversible, whereas late-stage RF is irreversible and involves the replacement of healthy tissue with excess fibrotic tissue, leading to debilitating functional decline.[8] Early detection during treatment (1-4 weeks) is desirable, potentially allowing for intervention, such as treatment plan alteration or administration of pharmaceuticals that may mitigate RILI without sacrificing treatment effectiveness.[4,5,9,10]

During treatment planning, cumulative dose to healthy tissue (dose-volume histograms, mean lung dose) is used to minimize RILI, but suffers from low predictive power.[3,4,11-13] Pulmonary function tests (PFTs) may be used during and after RT to determine lung function. Unfortunately, PFTs only offer global measurements and typically modestly change as a result of RILI, with some patients exhibiting symptoms without accompanying declines in PFTs.[3,4,14,15] Radiographic techniques tend to be insensitive to the early functional lung changes associated with acute RP. Anatomical changes associated with different lung densities are typically not observed until after completion of RT,[2,16-18] at which point RILI may be irreversible.

Hyperpolarized noble gases (eg, $^{3}$He, $^{129}$Xe) show promise for functional lung magnetic resonance imaging (MRI) by boosting the detectable signal by a factor of approximately $10^{4}$.[19] Hyperpolarized $^{3}$He and $^{129}$Xe MRI of the airspaces have previously been investigated for RILI detection in rats and humans.[20-22] The solubility of xenon allows for detection of a $^{129}$Xe signal within various tissue compartments beyond airspaces such as the lung parenchyma, blood plasma, and red blood cells (RBCs), among others (eg, lipids, brain), giving $^{129}$Xe a significant advantage.[19,23,24] The exchange of xenon into these compartments is sensitive to changes in compartmental structure and function, such as compartment size and gas exchange. Dissolved-phase $^{129}$Xe MRI has previously been investigated in animal models of RILI.[25,26] Furthermore, time-resolved measurements of these signals have demonstrated gas exchange reductions between these compartments following irradiation of the lung.[27-29] Changes to the RBC compartment resulting from RILI measurable with dissolve-phase $^{129}$Xe MRI have not as yet been correlated with quantitative histology of RBC distribution after irradiation, however. Previous studies also used whole-thorax or hemithoracic irradiation schemes that likely caused additional damage (eg, heart, diaphragm), potentially confounding conclusions drawn from imaging results.

The purpose of this proof-of-concept study was to perform hyperpolarized $^{129}$Xe chemical shift imaging (CSI) in rat lungs and measure changes in lung tissue and RBC signals following partial-lung irradiation, compared with nonirradiated age-matched rats. Imaging results are correlated with quantitative histology of both pulmonary tissue (PT) and RBC distribution to confirm RP and changes to perfusion, allowing for the investigation of the physiological source of the observed changes in $^{129}$Xe signals.

## Methods

### Animal preparation and irradiation

All animal experiments were approved by the Animal Care Committee at University Health Network, following Canadian Council on Animal Care guidelines. Two age-matched cohorts of male Sprague-Dawley rats (Charles River Laboratories, Saint-Constant, QC) were used. One cohort was irradiated using an image-guided small animal irradiator (X-Rad 225Cx, PXi, North Brantford, CT). A partial volume of the right medial lung was irradiated using a $1 \times 1$ cm$^2$ collimated beam, avoiding the heart and diaphragm (Fig 1). Anatomical features were used for targeting the same volume in each rat. A single dose of 20-Gy photons (225 kVp, 13 mA, 2.28 Gy/min at 1.5 cm of solid water) was delivered.[30,31] Ten Gray were delivered anteroposterior followed by a 10-Gy posteroanterior dose. Dose calculation and visualization were performed in SmART-Plan (Precision X-Ray, North Brantford, CT) and Raystation (RaySearch Laboratories, Stockholm, Sweden), respectively. After irradiation, the rats were incubated for 4 weeks, allowing RILI to manifest. This irradiation scheme ensured the presence of RILI based on pilot irradiations involving several doses and incubation periods. Histological evidence of RILI in this pilot cohort confirmed the irradiation scheme would produce a measurable effect potentially detectable by imaging. The cohort sizes were 6 rats each because 1 nonirradiated rat exhibited damage to both lungs consistent with ventilator-induced lung injury and was excluded. The mean weights were $497 \pm 38$ g and $485 \pm 13$ g for the irradiated and

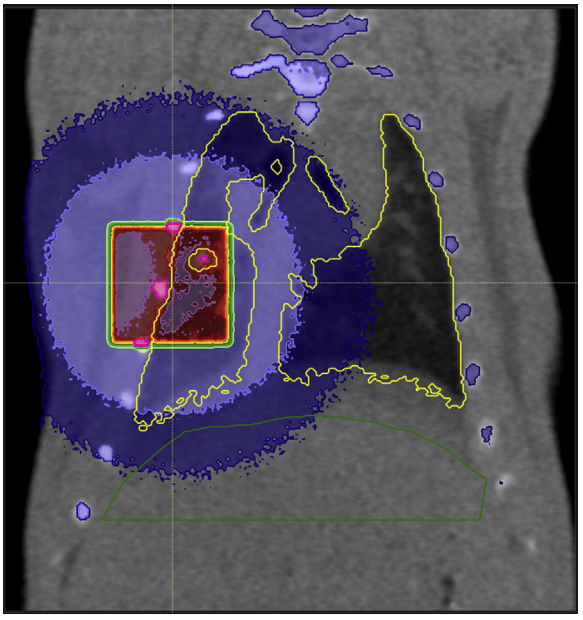

**Figure 1** Example irradiation treatment plan with cone beam computed tomography scan in the coronal view. Red indicates isodose of 95% of total dose (20 Gy), green indicates 50% of dose (treated volume), light purple indicates 2% of dose, and dark purple indicates 1% of dose. Yellow line indicates the lung contours.

nonirradiated cohorts, respectively. The animals were prepared and ventilated for MRI as described previously.[27] Medical air was used to ventilate the rats during imaging with supplementary 100% $O_2$ briefly supplied (1-2 minutes) to an animal if oxygen saturation did not recover to baseline after a breathhold. Oxygen saturation was monitored with preclinical monitoring equipment (model 1030, SA Instruments Inc., Stony Brook, NY).

## Two-dimensional CSI

Imaging was performed on a clinical 1.5T MRI system (Signa HDxt, GEHC, Waukesha, WI) with a transmit/receive birdcage rat coil (Morris Instruments, Ottawa, ON). A 2-dimensional CSI (2DCSI) sequence (field of view = $5 \times 5$ cm$^2$, matrix size = $8 \times 8$, repetition time = 180 ms, BW = $\pm$4 kHz, 256 spectral points) was used to acquire localized spectra in the coronal plane encompassing the rat thorax during a 13-second breath-hold. Additional details regarding acquisition and reconstruction can be found in Appendix E1, available as supplementary material online only at www.advancesradonc.org.

## Histology

Immediately following each imaging experiment, the rats were euthanized and the lungs were removed, with blood deliberately retained by ligation of major vessels. Extraction and filling of the lungs was accomplished within approximately 20 minutes postmortem. The lungs were then fixed and 5-μm sections were taken from the middle of the lung in the coronal plane and stained with hematoxylin and eosin. For each rat, 50 images (15 basal, 25 medial, 10 apical) were captured in Pannoramic Viewer (3DHistech, Budapest, Hungary) at 20× magnification (865 × 600 μm) from each lung (right and left). Images were segmented into airspaces, PT, and RBCs using a k-means algorithm in MATLAB (MathWorks, Natick, MA), similar to previous work.[32] The number of image pixels within tissue and RBC clusters divided by the total image pixels was computed to yield measurements of relative PT and RBC distribution, defined as percent tissue area (PTA) and percent RBC area (PRA), respectively.[33] Changes to PTA and PRA reflect bulk changes in PT and RBCs respectively, affecting gas exchange. The mean and standard deviation of PTA and PRA were also calculated for each lung (right and left) of each animal of both cohorts. The right-to-left (R/L) lung ratios of the means and standard deviations for PTA and PRA were calculated (defined as $\kappa_{PTA}$, $\kappa_{PRA}$, $\eta_{PTA}$, and $\eta_{PRA}$). Additional details regarding histology preparation and segmentation can be found in the supplementary materials.

## Image analysis

Regions of interest (ROIs) were chosen to separate right and left lungs based on the gas-phase images, avoiding nonlung regions (eg, heart, great vessels) that could be present in tissue and RBC images. The mean tissue and RBC signal ($S_T$ and $S_{RBC}$) in the ROIs were measured in both lungs. Additionally, the signals for each ROI were binned into a histogram consisting of 20 bins. The full-width at half-maximum (FWHM) of each histogram was calculated as a measure of signal heterogeneity for both compartments ($FWHM_T$ and $FWHM_{RBC}$). The R/L lung ratios of $S_T$, $S_{RBC}$, $FWHM_T$, and $FWHM_{RBC}$ were calculated as measures of regional asymmetry (abbreviated $\kappa_T$, $\kappa_{RBC}$, $\eta_T$, and $\eta_{RBC}$, respectively). These ratios removed variations resulting from systematic differences within and between animals, such as variations in organwide lung function or anatomy. Thus, $\kappa$ and $\eta$ values less than or greater than unity denoted increased signal asymmetry resulting from irradiation between the right and left lungs.

Statistical analyses were performed using Prism (GraphPad Software, San Diego, CA). Two-tailed $t$ tests characterized differences in $\kappa_T$ and $\kappa_{RBC}$ between cohorts. The same test was used for histological measurements of $\kappa_{PTA}$, $\kappa_{PRA}$, $\eta_{PTA}$, and $\eta_{PRA}$; however, CSI measurements of $\eta_T$ and $\eta_{RBC}$ were observed to have non-normal distributions (Shapiro-Wilk). As a result, a nonparametric, a 2-tailed Mann-Whitney $U$ test was performed. Significantly different spectroscopic and histological results were analyzed using 2-tailed, nonparametric Spearman

correlation. All statistical tests were performed with a 95% confidence level. The image analyst (B.Z.) was blinded to which rats had been irradiated until after analysis.

## Results

### Two-dimensional CSI

Figure 2(B-D) shows representative projection images for gas, tissue, and RBC from a healthy rat. Figure 2(E-H) show normalized tissue and RBC images from representative nonirradiated and irradiated rats. $S_T$ was observed to increase in the irradiated lung in the vicinity of irradiation and in regions away from the radiation field (Fig 2G, arrow 1) compared with the nonirradiated rat. Increases were also observed in the contralateral lung, but to a lesser extent. $S_{RBC}$ was observed to vary significantly in the irradiated lung, some with increases observed in the region of irradiation (Fig 2H, arrow 2).

Figure 3 summarizes CSI results. Measurements of $\kappa_T$ were significantly increased ($P < .01$) in the irradiated cohort compared with the nonirradiated cohort with mean values of $1.181 \pm 0.134$ and $0.984 \pm 0.055$, respectively, indicating increased signal intensity in the right lung of the irradiated cohort. $\kappa_{RBC}$ slightly increased in the irradiated cohort compared with the nonirradiated cohort with mean values of $1.138 \pm 0.196$ and $0.942 \pm 0.118$, respectively, although this difference was not significant ($P = .0586$). Considering signal heterogeneity, $\eta_T$ was significantly increased ($P < .05$) in the irradiated cohort compared with the nonirradiated cohort with mean values of $1.599 \pm 1.173$ and $0.562 \pm 0.358$, respectively. Similarly, $\eta_{RBC}$ was significantly increased in the irradiated cohort ($P < .01$) with mean values of $1.493 \pm 0.642$ and $0.763 \pm 0.173$ for the irradiated and nonirradiated cohorts, respectively.

### Histology

Lung tissue extracted from irradiated animals confirmed regional RP. Figure 4 shows representative micrographs from the right lung of an irradiated rat, including images within and outside of the irradiation field. Evidence of an inflammatory response within the beam portal was observed, including edema, thickening of alveolar interstitium, and presence of infiltrating macrophages. The damage to PT was very heterogeneous (Fig 4). Within the radiation field, patchy areas of tissue thickening were observed alongside areas of tissue reduction. Example segmentation from the right lungs of both cohorts can be found in the supplementary materials. Irradiated tissue was characterized by a distinct reduction of RBCs in the radiation field.

Figure 5 summarizes quantitative histological results. $\kappa_{PRA}$ was observed to be significantly decreased ($P < .01$) in the irradiated cohort compared with the nonirradiated cohort with mean values of $0.518 \pm 0.126$ and $0.948 \pm 0.264$, respectively. $\eta_{PRA}$ was observed to be slightly increased in the irradiated animals, although this difference was not significant, with mean values of $1.635 \pm 0.464$ and $1.054 \pm 0.627$ for the irradiated and nonirradiated cohorts, respectively. In the irradiated lungs, increases in PTA resulting from RP appeared to offset decreases in PTA because of tissue destruction; as a result, $\kappa_{PTA}$ was observed to be only slightly increased in the irradiated cohort compared with the nonirradiated cohort, with means of $1.079 \pm 0.125$ and $0.987 \pm 0.080$, respectively. This same heterogeneous tissue damage significantly increased $\eta_{PTA}$ ($P < .0001$) in the irradiated cohort compared with the nonirradiated cohort, with means of $3.306 \pm 0.646$ and $1.090 \pm 0.241$, respectively. Figure 5E shows a negative correlation between $\eta_{RBC}$ and $\kappa_{PRA}$ ($r = -0.643$, $P < .05$). Qualitatively good separation was also observed between $\kappa_T$ and $\eta_{PTA}$, although this was not significant ($r = 0.483$, $P > .05$) because of a single irradiated rat that did not exhibit a response on CSI. Clustering was also observed between $\eta_T$ and $\eta_{PTA}$; however, this result was not quite significant ($r = 0.566$, $P = .0591$). No other correlations were observed.

## Discussion

This work confirms that CSI of hyperpolarized $^{129}Xe$ can be used to detect regional $S_T$ and $S_{RBC}$ changes at 4 weeks postirradiation in a rat model of RILI involving partial-lung irradiation. Significantly increased $S_T$ asymmetry ($\kappa_T$) between the right and left lungs was observed after irradiation. This is consistent with other studies that report increased $S_T$ because of inflammation associated with RP.[27-29] This was accompanied by significantly increased asymmetric $S_T$ heterogeneity ($\eta_T$). These results were confirmed histologically with increased PT heterogeneity in the irradiated lung ($\eta_{PTA}$).

Histology of RBC distribution was included to evaluate any observed perfusion changes that may indicate damage to the vasculature. This is the first time to our knowledge that RBC distribution has been included alongside imaging results. The histologically determined RBC asymmetry parameter ($\kappa_{PRA}$) was significantly decreased, indicating decreased amounts of blood in the irradiated right lung localized in the irradiated region (Fig 4A,C,D). From imaging, increased asymmetric $S_{RBC}$ heterogeneity in the irradiated right lung ($\eta_{RBC}$) was shown to correlate with decreasing $\kappa_{PRA}$ (Fig 5E); however, $\kappa_{RBC}$ as measured by CSI was not significantly different indicating unchanged overall $S_{RBC}$ intensity. This could possibly be explained by a compensatory effect of the lungs to focal injury, such as an increase in perfusion to healthy regions. PRA calculated in the right lung using micrographs acquired from outside the

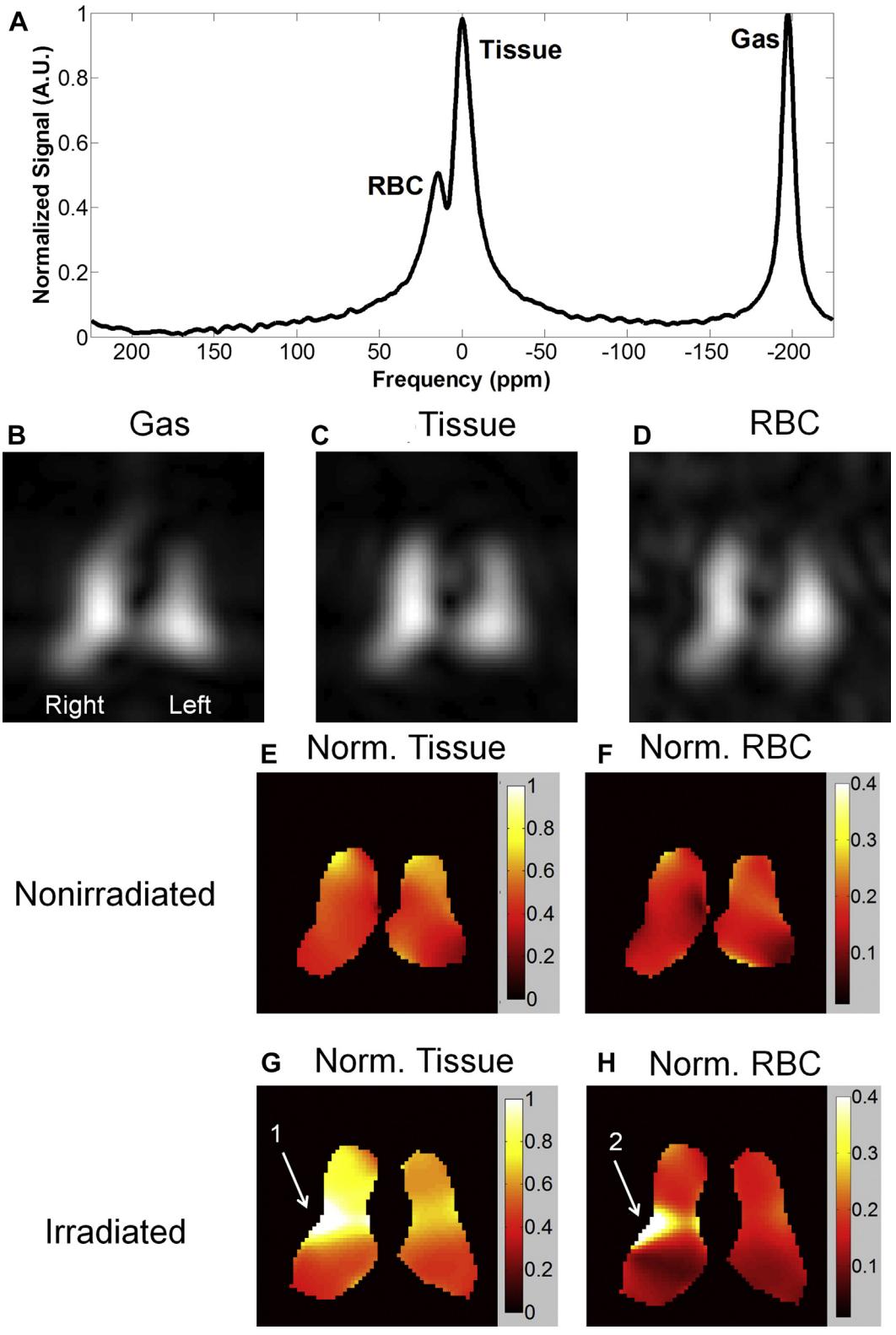


**Figure 2** (A) Representative whole-lung $^{129}$Xe magnitude spectrum from nonirradiated rat lung. Representative 2-dimensional chemical shift imaging images from a nonirradiated rat showing all 3 compartments (B-D). Corresponding segmented tissue and red blood cell (RBC) images normalized by gas images for a representative nonirradiated (E, F) and irradiated (G, H) rat. Arrow 1 indicates increased tissue signal in the irradiated (right) compared with the contralateral (left) lung. Arrow 2 indicates increased RBC signal in the region of irradiation (medial).

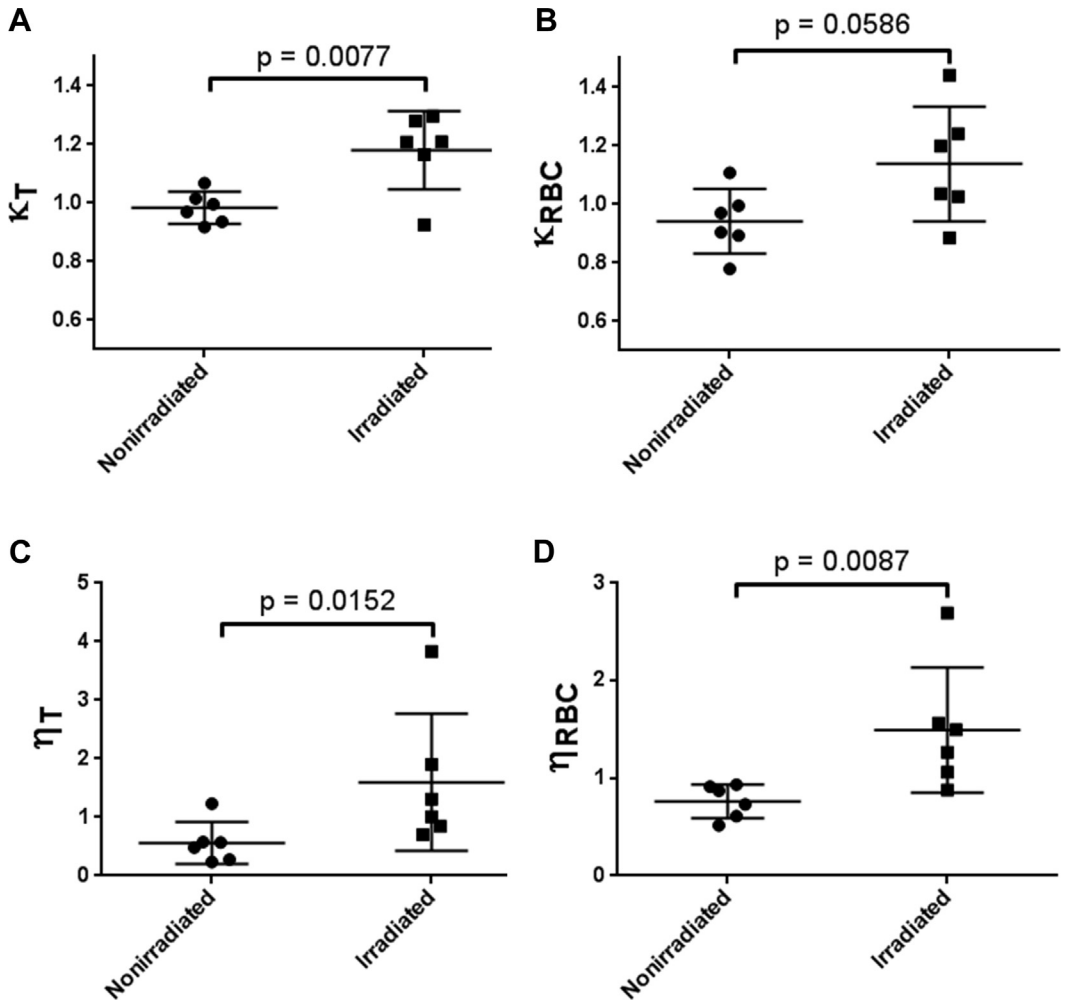


**Figure 3** Two-dimensional chemical shift imaging measurements of right-to-left asymmetry. Top row shows asymmetric signal intensity parameter (κ) in the (A) pulmonary tissue (PT) and (B) red blood cell (RBC) compartments. Bottom row shows asymmetric signal heterogeneity parameter (η) in the (C) PT and (D) RBC compartments.

radiation field showed a slight increase to 9.39% ± 4.53% in the irradiated cohort from 5.20% ± 3.56% in the nonirradiated cohort, although this was not significant (*t* test, $P > .05$). Acute, short-lived increases in perfusion after irradiation in the irradiated lung have been previously reported in rats.[34-36] These increases may counteract reductions in $S_{RBC}$ associated with reduced amounts of RBCs contributing to less signal intensity asymmetry between lungs. Curiously, several rats exhibited an increase in $S_{RBC}$ near the region of irradiation, despite histologically measured RBC decreases (Fig 2H, arrow 2). This could possibly be explained by increased time spent in the gas exchange region ($t_x$) resulting from vessel occlusion in injured areas, allowing more time for $^{129}$Xe to accumulate within the RBC compartments, counteracting reductions in the numbers of RBCs present for exchange, and/or inhibited transfer of $^{129}$Xe. Increased $t_x$ has been previously reported in an animal model.[28] Nevertheless, further investigation is required, and these images should be interpreted with caution as the low in-plane spatial resolution and lack of coronal localization likely contributed partial-volume effects, potentially obscuring and/or averaging regions of signal increase or decrease, especially in regions bordering the radiation field. In the future, higher spatial resolution, multislice, or 3-dimensional acquisitions should alleviate these concerns. Additionally, staining for specific structure/cell types (ie, capillary endothelium) may allow for the determination of the physiological source of observed perfusion decreases.

Measurements of $S_T$ and $S_{RBC}$ heterogeneity were highly asymmetric (increased heterogeneity in right lung) in irradiated animals; however, nonirradiated animals exhibited less dramatic asymmetry in the opposite direction. $\eta_T$ and $\eta_{RBC}$ were notably less than unity in healthy rats, suggesting inherent signal heterogeneity in the left lung (Fig 3C, 3D) that was not reflected histologically. Presumably this reflects natural anatomical asymmetries present in the rat (eg, sizes differences between lungs, position of heart/great vessels) that may be present in

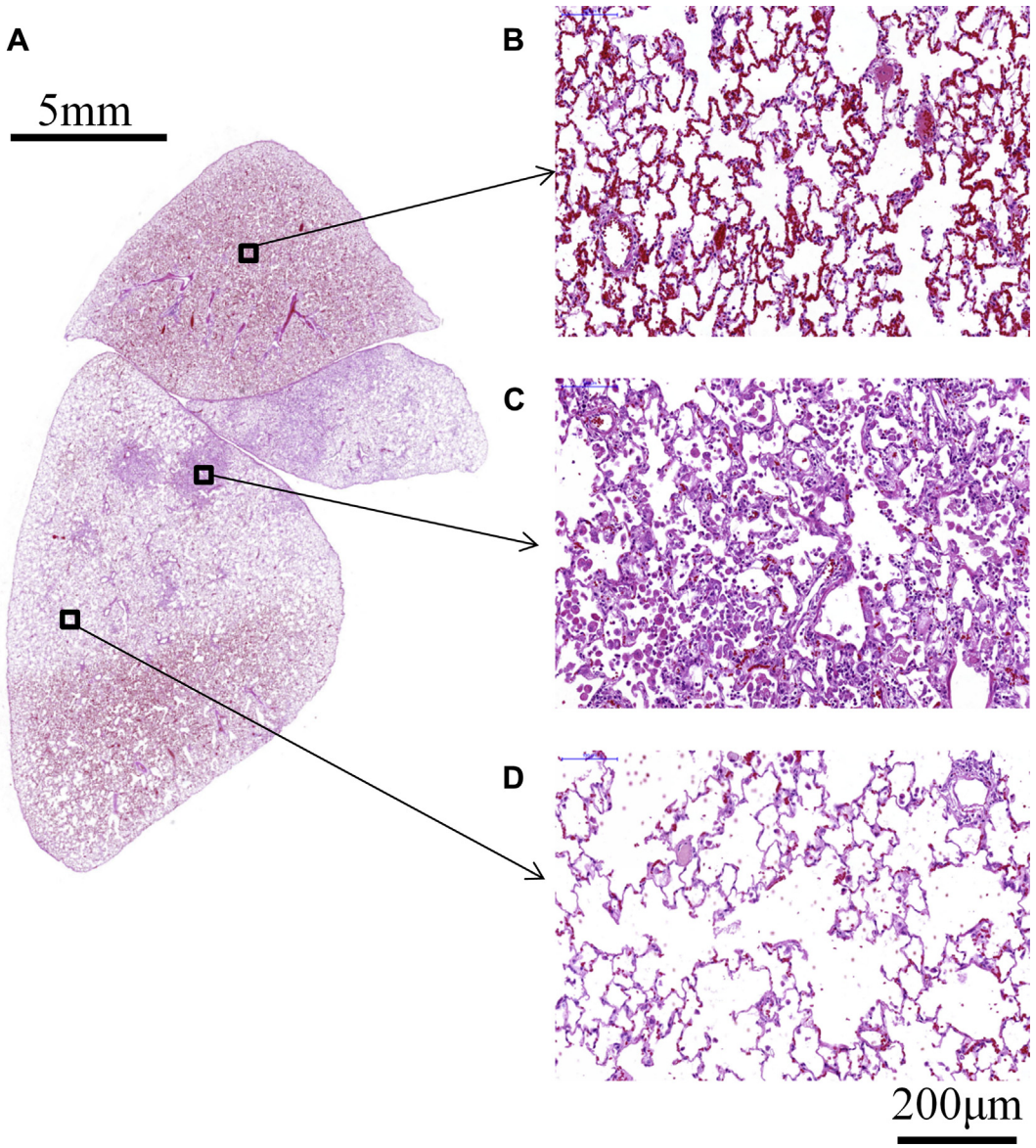


**Figure 4** (A) Coronal tissue section of the right lung from a representative irradiated rat with evidence of radiation-induced lung injury. (B-D) Different regions of damage at 20× magnification emphasizing the heterogeneous nature of the injury. (B) Regions outside the radiation field were characterized by moderate radiation pneumonitis and significant red blood cells. The lung regions within the radiation field were characterized by tissue thickening (C) as well as airway destruction and a loss of tissue (D). All regions within the beam portal had significantly decreased red blood cells (C, D) compared with regions outside.

images despite ROI segmentation resulting from the acquisition of projections. These additional sources of signal may contribute to the increased signal inhomogeneity observed in the left lungs of nonirradiated rats.

In this focal irradiation model, use of image guidance spared adjacent organs, specifically the heart, avoiding cardiac injury that may affect RBC signal downstream from the heart in an uncontrolled manner. Irradiation of the heart is known to cause detrimental biological responses in animal studies.[37,38] Cardiac damage may be present in other $^{129}$Xe MRI animal studies involving whole or hemithoracic irradiation,[27-29] potentially confounding imaging results with their physiological source (cardiac damage, pulmonary damage, or both). Additionally, the small volume irradiated in this study (~0.5 mL, $V_{20}$ approximately 10%) tested the sensitivity of dissolved-phase $^{129}$Xe to decreased levels of damage than whole or hemithoracic irradiation because biological insult depends on the volume of lung irradiated in both rats and humans.[3,4,39-41] Although the single dose/volume nature of the irradiation scheme used limits the clinical relevance of this work by mimicking damage that is likely representative of injury following a full treatment plan, the presented partial-lung irradiation rat model, associated MRI methodology, and histological analysis

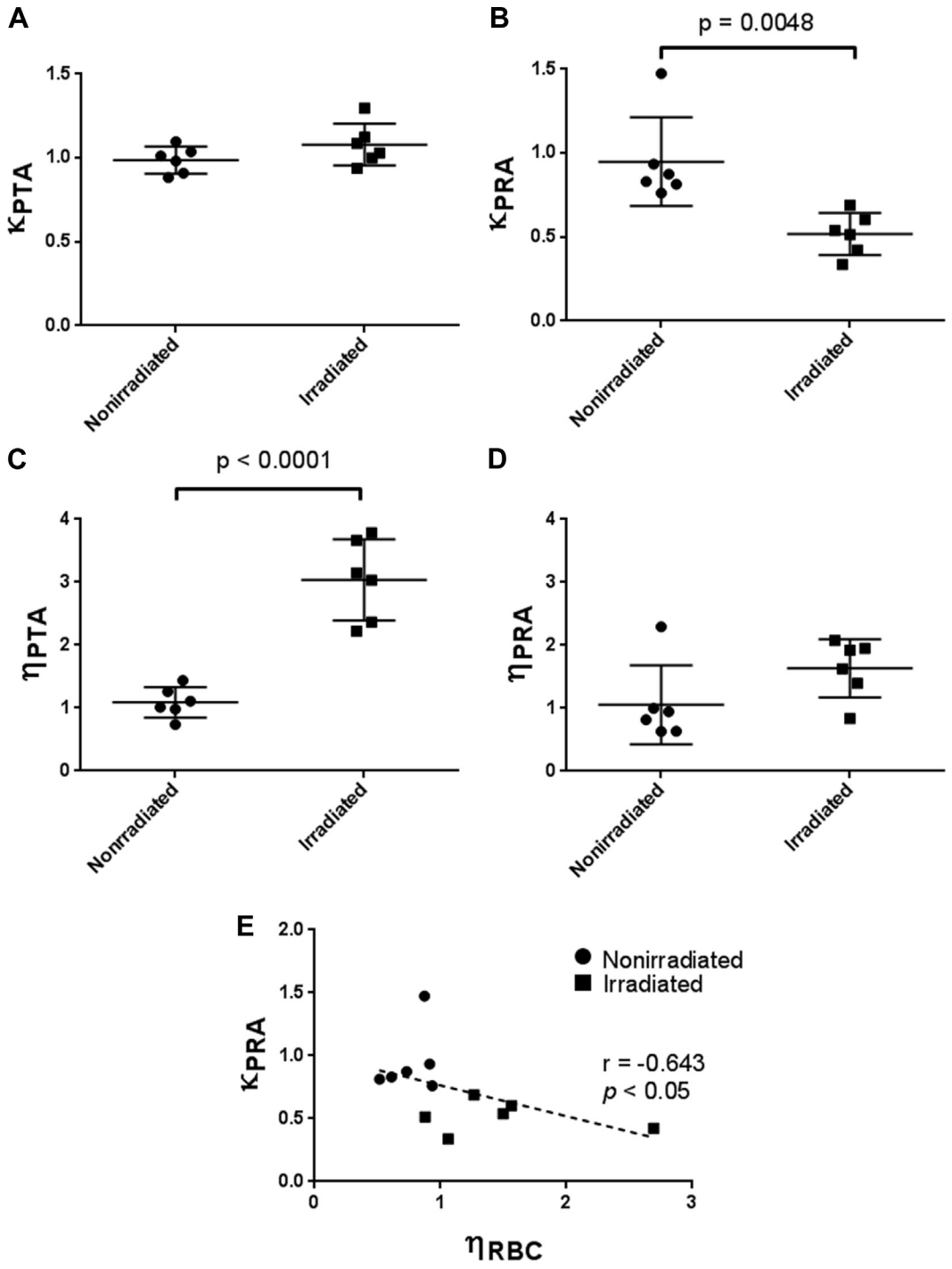


**Figure 5** Quantitative histological results showing measurements of regional asymmetry of relative pulmonary tissue and red blood cell (RBC) distribution (A, B) and heterogeneity (C, D). (E) Spearman correlation of $\eta_{RBC}$ and $\kappa_{PRA}$ illustrating increasing RBC signal heterogeneity in the right lung with decreasing RBC distribution. The dashed line is a linear fit to guide the eye.

will provide a useful platform for future animal studies of RILI. These could include implementation of a fractionated RT plan, incorporating several dose and volume groups, to better simulate clinical therapy. These experimental groups, in conjunction with dissolved-phase $^{129}$Xe MRI, may be useful to evaluate the effectiveness of different treatment schemes and answer important radiobiological questions about radiation toxicity in the lung. For example, the emerging practice of stereotactic body RT for inoperable lung cancers may benefit from preclinical studies investigating lung toxicity in comparison to conventional treatment.[42] Additionally, imaging at

multiple time points before, during, and after irradiation could assist in the development of predictive biomarkers that may be used to guide therapy and improve overall understanding of the proliferation of RILI.

It is important to recognize that our images represent the density of $^{129}$Xe in tissue and RBC compartments that accumulates because of exchange from airspaces in a single gas exchange time of 180 ms and do not convey gas exchange information directly. By acquiring images at multiple exchange times, signals are sensitized to the uptake of $^{129}$Xe between compartments and can be analyzed using physiological models to obtain compartment sizes, barrier thicknesses, and transfer times.[43-45] Increases in gas exchange transfer times and PT thicknesses were reported in separate studies 2 weeks and 3 months, respectively, after whole-thorax irradiation using spectroscopy.[27,28] Imaging 2 weeks after hemithoracic irradiation showed increased tissue thickness and decreased relative blood volume in the irradiated lung.[29] Future studies involving this irradiation model will benefit from the incorporation of gas exchange measurements; however, it is significant that functional changes associated with RP are detectable in a semiquantitative manner using compartmental signal intensities and heterogeneities along with comparison to the contralateral lung.

Similar compartmentally dissolved $^{129}$Xe MRI has previously been performed in healthy humans and patients with asthma, interstitial lung disease, and chronic obstructive pulmonary disease.[46-49] Future work involving longitudinal imaging of human RT patients would be beneficial for investigating the ability of dissolved-phase $^{129}$Xe MRI to detect functional and structural changes associated with RILI.

## Conclusion

This work demonstrates the feasibility of dissolved-phase hyperpolarized $^{129}$Xe CSI for regional detection of RILI. Specifically, dissolved $^{129}$Xe CSI signal intensity can detect regional asymmetries and heterogeneity of lung parenchymal tissue and RBC distribution consistent with quantitative histology in a partial-lung irradiation rat model of RILI 4 weeks after irradiation.

## Acknowledgments

The authors thank to Dr. Richard Hill and Dr. Ozkan Doganay for assistance with the irradiation scheme and magnetic resonance imaging methodology, respectively. The authors also recognize the Spatio-Temporal Targeting and Amplification of Radiation (STTARR) facility for assistance with irradiations. Special thanks to N. Kanhere, A. Lindenmaier, Y. Friedlander, and F. Morgado for assistance with imaging experiments.

## References

1. Gross N. The pathogenesis of radiation-induced lung damage. *Lung*. 1981;159:115.
2. Movsas B, Raffin TA, Epstein AH, Link CJ. Pulmonary radiation injury. *Chest*. 1997;111:1061-1076.
3. Marks LB, Yu X, Vujaskovic Z, Small W, Folz R, Anscher MS. Radiation-induced lung injury. *Semin Radiat Oncol*. 2003;13:333-345.
4. Mehta V. Radiation pneumonitis and pulmonary fibrosis in non-small-cell lung cancer: Pulmonary function, prediction, and prevention. *Int J Radiat Oncol Biol Phys*. 2005;63:5-24.
5. Tsoutsou PG, Koukourakis MI. Radiation pneumonitis and fibrosis: Mechanisms underlying its pathogenesis and implications for future research. *Int J Radiat Oncol Biol Phys*. 2006;66:1281-1293.
6. Ghafoori P, Marks L, Vujaskovic Z, Kelsey C. Radiation-induced lung injury: Assessment, Management, and Prevention. *Oncology*. 2008;22:37-47.
7. Ware LB. Pathophysiology of acute lung injury and the acute respiratory distress syndrome. *Semin Respir Crit Care Med*. 2006;27:337-349.
8. Yarnold J, Vozenin Brotons MC. Pathogenetic mechanisms in radiation fibrosis. *Radiother Oncol*. 2010;97:149-161.
9. Magana E, Crowell RE. Radiation pneumonitis successfully treated with inhaled corticosteroids. *South Med J*. 2003;96:521-524.
10. Delanian S, Lefaix JL. Current management for late normal tissue injury: Radiation-induced fibrosis and necrosis. *Semin Radiat Oncol*. 2007;17:99-107.
11. Hernando ML, Marks LB, Bentel GC, et al. Radiation-induced pulmonary toxicity: A dose-volume histogram analysis in 201 patients with lung cancer. *Int J Radiat Oncol Biol Phys*. 2001;51:650-659.
12. Rodrigues G, Lock M, D'Souza D, Yu E, Van Dyk J. Prediction of radiation pneumonitis by dose-volume histogram parameters in lung cancer - A systematic review. *Radiother Oncol*. 2004;71:127-138.
13. Madani I, De Ruyck K, Goeminne H, De Neve W, Thierens H, Van Meerbeeck J. Predicting risk of radiation-induced lung injury. *J Thorac Oncol*. 2007;2:864-874.
14. Lind PA, Marks LB, Hollis D, et al. Receiver operating characteristic curves to assess predictors of radiation-induced symptomatic lung injury. *Int J Radiat Oncol Biol Phys*. 2002;54:340-347.
15. Fan M, Marks LB, Lind P, et al. Relating radiation-induced regional lung injury to changes in pulmonary function tests. *Int J Radiat Oncol Biol Phys*. 2001;51:311-317.
16. Ikezoe J, Takashima S, Morimoto S, et al. CT appearance of acute injury in the lung. *AJR Am J Roentgenol*. 1988;150:765-770.
17. Jenkins P, Welsh A. Computed tomography appearance of early radiation injury to the lung: Correlation with clinical and dosimetric factors. *Int J Radiat Oncol Biol Phys*. 2011;81:97-103.
18. Choi YW, Munden RF, Erasmus JJ, et al. Effects of radiation therapy on the lung: Radiologic appearances and differential diagnosis. *Radiographics*. 2004;24:985-998.
19. Möller HE, Chen XJ, Saam B, et al. MRI of the lungs using hyperpolarized noble gases. *Magn Reson Med*. 2002;47:1029-1251.
20. Ward ER, Hedlund LW, Kurylo WC, et al. Proton and hyperpolarized helium magnetic resonance imaging of radiation-induced lung injury in rats. *Int J Radiat Oncol Biol Phys*. 2004;58:1562-1569.
21. Ireland RH, Din OS, Swinscoe JA, et al. Detection of radiation-induced lung injury in non-small cell lung cancer patients using hyperpolarized helium-3 magnetic resonance imaging. *Radiother Oncol*. 2010;97:244-248.
22. Ouriadov A, Fox M, Hegarty E, Parraga G, Wong E, Santyr GE. Early stage radiation-induced lung injury detected using hyperpolarized 129Xe morphometry: Proof-of-concept demonstration in a rat model. *Magn Reson Med*. 2016;75:2421-2431.

23. Sakai K, Bilek AM, Oteiza E, et al. Temporal dynamics of hyperpolarized 129Xe resonances in living rats. *J Magn Reson B*. 1996; 111:300-304.
24. Mugler JP, Driehuys B, Brookeman JR, et al. MR imaging and spectroscopy using hyperpolarized Xe-129 gas: Preliminary human results. *Magn Reson Med*. 1997;37:809-815.
25. Driehuys B, Raidy T, Pollaro J. Hyperpolarized 129Xe MRI for functional assessment of radiation-induced lung injury. *Int J Radiat Oncol Biol Phys*. 2005;63:460-461.
26. Ruppert K, Mata JF, Cai J, et al. Detecting radiation-induced lung injuries using XTC MRI: Initial findings. *Proc Intl Mag Reson Med*. 2007;15:3202.
27. Fox MS, Ouriadov A, Thind K, et al. Detection of radiation induced lung injury in rats using dynamic hyperpolarized 129Xe magnetic resonance spectroscopy. *Med Phys*. 2014;41:72302.
28. Li H, Zhang Z, Zhao X, Sun X, Ye C, Zhou X. Quantitative evaluation of radiation-induced lung injury with hyperpolarized xenon magnetic resonance. *Magn Reson Med*. 2016;76:408-416.
29. Doganay O, Stirrat E, McKenzie C, Schulte RF, Santyr GE. Quantification of regional early stage gas exchange changes using hyperpolarized 129Xe MRI in a rat model of radiation-induced lung injury. *Med Phys*. 2016;43:2410-2420.
30. Chair C-M, Coffey CW, DeWerd LA, et al. AAPM protocol for 40–300 kV x-ray beam dosimetry in radiotherapy and radiobiology. *Med Phys*. 2001;28:868-893.
31. Lindsay PE, Granton PV, Gasparini A, et al. Multi-institutional dosimetric and geometric commissioning of image-guided small animal irradiators. *Med Phys*. 2014;41:31714.
32. Sieren JC, Weydert J, Bell A, et al. An automated segmentation approach for highlighting the histological complexity of human lung cancer. *Ann Biomed Eng*. 2010;38:3581-3591.
33. Takahashi A, Hamakawa H, Sakai H, et al. Noninvasive assessment for acute allograft rejection in a rat lung transplantation model. *Physiol Rep*. 2014;2:e12244.
34. Ts'ao C, Ward WF, Port CD. Radiation injury in rat lung I. Prostacyclin PGl2 production, arterial perfusion, and ultrastructure. *Radiat Res*. 1983;96:284-293.
35. Ward WF, Solliday NH, Molteni A, Port CD. Radiation injury in rat lung II. Angiotensin-converting enzyme activity. *Radiat Res*. 1983; 96:294-300.
36. Ts'ao C, Ward WF, Port CD. Radiation Injury in rat lung III. Plasminogen activator and fibrinolytic inhibitor activities. *Radiat Res*. 1983;96:301-308.
37. van Luijk P, Novakova-Jiresova A, Faber H, et al. Radiation damage to the heart enhances early radiation-induced lung function loss. *Cancer Res*. 2005;65:6509-6511.
38. Novakova-Jiresova A, van Luijk P, van Goor H, Kampinga HH, Coppes RP. Pulmonary radiation injury: Identification of risk factors associated with regional hypersensitivity. *Cancer Res*. 2005;65: 3568-3576.
39. Novakova-Jiresova A, van Luijk P, van Goor H, Kampinga HH, Coppes RP. Changes in expression of injury after irradiation of increasing volumes in rat lung. *Int J Radiat Oncol Biol Phys*. 2007; 67:1510-1518.
40. van Luijk P, Novakova-Jiresova A, Faber H, et al. Relation between radiation-induced whole lung functional loss and regional structural changes in partial irradiated rat lung. *Int J Radiat Oncol Biol Phys*. 2006;64:1495-1502.
41. Marks LB, Bentzen SM, Deasy JO, et al. Radiation dose–volume effects in the lung. *Int J Radiat Oncol Biol Phys*. 2015;76:S20-S27.
42. Timmerman RD, Park C, Kavanagh BD. The North American experience with stereotactic body radiation therapy in non-small cell lung cancer. *J Thorac Oncol*. 2006;2:2-5.
43. Månsson S, Wolber J, Driehuys B, Wollmer P, Golman K. Characterization of diffusing capacity and perfusion of the rat lung in a lipopolysaccharide disease model using hyperpolarized 129Xe. *Magn Reson Med*. 2003;50:1170-1179.
44. Patz S, Muradyan I, Hrovat MI, et al. Diffusion of hyperpolarized 129Xe in the lung: A simplified model of 129Xe septal uptake and experimental results. *New J Phys*. 2011;13.
45. Chang YV. MOXE: A model of gas exchange for hyperpolarized 129Xe magnetic resonance of the lung. *Magn Reson Med*. 2013;69: 884-890.
46. Mugler JP III, Altes TA, Ruset IC, et al. Simultaneous magnetic resonance imaging of ventilation distribution and gas uptake in the human lung using hyperpolarized xenon-129. *Proc Natl Acad Sci U S A*. 2010;107:21707-21712.
47. Cleveland ZI, Cofer GP, Metz G, et al. Hyperpolarized Xe MR imaging of alveolar gas uptake in humans. *PLoS One*. 2010;5:e12192.
48. Qing K, Ruppert K, Jiang Y, et al. Regional mapping of gas uptake by blood and tissue in the human lung using hyperpolarized xenon-129 MRI. *J Magn Reson Imaging*. 2014;39:346-359.
49. Kaushik SS, Robertson SH, Freeman MS, et al. Single-breath clinical imaging of hyperpolarized 129xe in the airspaces, barrier, and red blood cells using an interleaved 3D radial 1-point Dixon acquisition. *Magn Reson Med*. 2016;75:1434-1443.